Ductile Titanium Alloy with Low Poisson's Ratio

Y. L. Hao,* S. J. Li, B. B. Sun, M. L. Sui, and R. Yang

Shenyang National Laboratory for Materials Science, Institute of Metal Research, Chinese Academy of Sciences, 72 Wenhua Road, Shenyang 110016, China

(Received 28 January 2007; published 25 May 2007)

We report a ductile β-type titanium alloy with body-centered cubic (bcc) crystal structure having a low Poisson's ratio of 0.14. The almost identical ultralow bulk and shear moduli of ~24 GPa combined with an ultrahigh strength of ~0.9 GPa contribute to easy crystal distortion due to much-weakened chemical bonding of atoms in the crystal, leading to significant elastic softening in tension and elastic hardening in compression. The peculiar elastic and plastic deformation behaviors of the alloy are interpreted as a result of approaching the elastic limit of the bcc crystal under applied stress.

DOI: 10.1103/PhysRevLett.98.216405 PACS numbers: 62.20.Dc, 61.82.Bg, 61.82.Rx, 68.35.Rh

Poisson's ratio is an elastic coefficient that provides insight into chemical bonding of atoms regarding the variations of bond angle and bond length. From the elastic relations $\nu = (E/2G) - 1$ and $B = E/[3(1-2\nu)]$ (where ν, B, G, and E denote the Poisson's ratio, bulk, shear, and Young's modulus, respectively) it is immediately clear that if $B = G$ then $\nu = \frac{1}{8}$. One way of classifying solids is to plot their bulk modulus against shear modulus (Fig. 1): Above the solid line, the resistance to bond-length change exceeds that to bond-angle change, and vice versa. Although almost all metallic materials have positive Poisson's ratio of $\sim\frac{1}{3}$, there are still vast materials with low and even negative values [1]. Examples are given in Fig. 1 such as layered metal-like ceramics $M_{N+1}AX_N$ with low Poisson's ratio of $\sim\frac{1}{5}$ and beryllium with ultralow value of $\sim\frac{1}{20}$ [2,3].

In spite of the lack of a direct link between elastic properties and plastic deformation behavior, phenomenologically it is generally accepted that materials with low Poisson's ratio are brittle [4,5]. For example, ductile face-centered cubic metals have high Poisson's ratio, whereas brittle bcc metals have low values [6]. Although beryllium qualifies as metallic based on conductivity, it fails to show the usual metallic properties [2]. Achieving high Poisson's ratio has even been considered as a means to improve toughness of bulk metallic glass (BMG) [4]. The above standpoint, however, does not imply that the materials with high Poisson's ratio should be ductile, as evidenced by a large group of brittle ordered intermetallic compounds with high Poisson's ratio [5].

Here we report a β-type titanium alloy which qualifies as a new type of solid in terms of elastic property and plastic behavior. Of all known structural metals its low Poisson's ratio is second only to beryllium and close to $\frac{1}{8}$ (Fig. 1), but it exhibits an elongation of ~17% and area reduction of ~70% at room temperature as well as an extensibility of at least 3200% during cold rolling [7]. The alloy has a bulk modulus lower than most metals but a high strength of ~0.9 GPa. The excellent superelastic and nanostructure-forming capacities of the alloy render it useful in a range of applications such as orthopedic implant, high-damping structure, rubberlike metal foils, and high-strength metal sheets [7].

Ingots with diameter of 140 mm were made by vacuum arc melting, hot forged at 1273 and 1123 K to bars with diameter of 25 mm. Nominal chemical compositions of the ingots are $TiNb_{24}Zr_4$-based with 7.6, 7.8, 7.9, 8.0, and 8.1 Sn (weight percent, obtained by wet chemical analysis, same below). The oxygen contents (by gas analysis) are 0.12 for all except the 7.6 wt.% Sn alloy for which it is 0.07. These alloys have a β-transus at ~950 K. Uniaxial tensile and compression tests were conducted at room temperature with strain rates of 1.3×10^{-4} s^{-1} and 1 s^{-1}, respectively. Young's modulus E and shear modulus G were measured by free resonant vibration method according to Chinese standard GB/T2105-91 using samples 10 mm in diameter and 180 mm in length. These quantities (in GPa) were calculated from $E = 1.6067 \times 10^{-9} ml^3 f^2/d^4$ and $G = 5.093 \times 10^{-9} mlf_1^2/d^2$, where m, l, and d are the weight (g), length, and diameter (mm) of samples, and f and f_1 are resonance frequencies (Hz) of samples under bending and torsion condition, respectively. Poisson's ratio ν and bulk

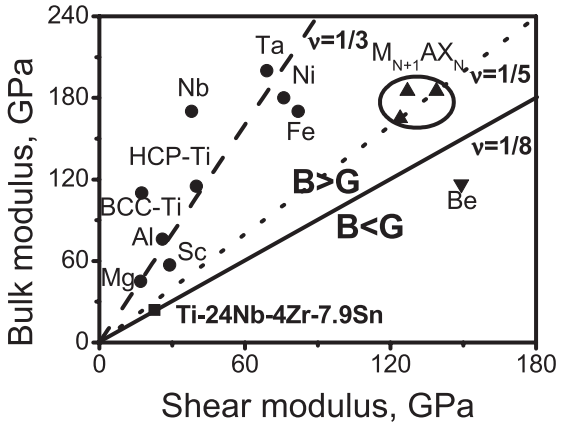

FIG. 1. Summary of shear and bulk moduli of some metals and metal-like ceramics $M_{N+1}AX_N$ in comparison with the present alloy.

modulus B were calculated from the elastic relations. The method has maximum system errors less than $\pm 1\%$ for E and G and $\pm 10\%$ for ν of absolute values. Microstructure was revealed by transmission electron microscopy (TEM).

Figure 2 shows the variations of elastic modulus and Poisson's ratio with Sn contents of the as-forged $TiNb_{24}Zr_4$-based alloys with bcc crystal structure. It is clear that both Young's and shear moduli change slightly in the studied chemical range and reach a minimum and maximum, respectively, in the alloy with 7.9 wt.% Sn alloy whereas Poisson's ratio and bulk modulus vary significantly with Sn contents and reach their minima with values 0.14 and 23.9 GPa, respectively. Additional measurements showed that Poisson's ratio is also sensitive to phase constitution and oxygen contents. Aging in the $(\alpha + \beta)$ two-phase field at 773 K for 1 h increases ν from 0.29 to 0.41 of the 7.6 wt.% Sn alloy with 0.07 oxygen while ν of the 8.0 wt.% Sn alloy reaches 0.32 from 0.25 with the increase of oxygen from 0.12 to 0.20. Such a large variation is quite different from most bulk materials which have almost constant value of ν.

The almost identical bulk and shear moduli of $TiNb_{24}Zr_4Sn_{7.9}$ alloy (~24 GPa, see Fig. 2) are ultralow compared to other metallic materials (Fig. 1), suggesting very weak and very similar elastic resistance to the change of both lattice spacing and lattice angle in the bcc crystal. A notable property of the studied alloy in comparison with other bulk metallic materials with low elastic modulus (e.g., Mg) is that it possesses much higher tensile strength [~0.9 GPa, see Fig. 3(a)]. Such a high strength combined with low elastic modulus suggests that the elastic limit of the bcc crystal may be approached under an applied stress. Theoretical investigation of elastic instability of perfect cubic crystal under external stress suggests the approaching of elastic limit due to softening of shear or bulk modulus can be triggered in succession [8]. The gradual elastic softening with the increase of applied stress would induce nonlinear elastic deformation in the absence of a reversible martensitic transformation (MT).

Figure 3(a) showed that the 7.9 wt.% Sn alloy exhibits nonlinear elasticity as well as softening and partial recovery of Young's modulus during uniaxial cyclic tensile test. For example, tensile Young's modulus decreased from ~42 GPa to ~20 GPa after 6% prestrain and then partially recovered to ~33 GPa after the release of internal stress at room temperature without loading [7]. The influence of internal stress on Young's modulus has been confirmed by additional measurement. High temperature annealing in the β-phase field increases tensile E from the original value of ~42 GPa to ~50 GPa [7]. Dynamical E can be

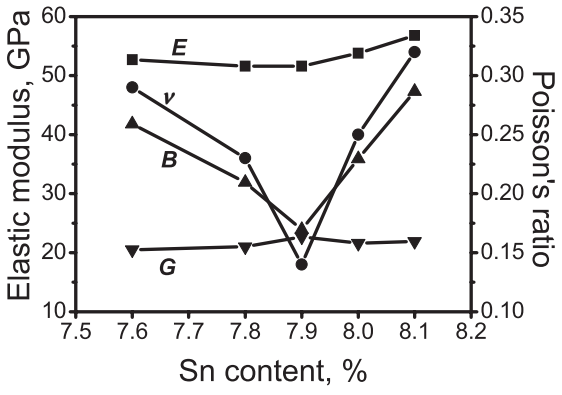

FIG. 2. Variations of elastic coefficients with Sn contents in $TiNb_{24}Zr_4$-based alloys.

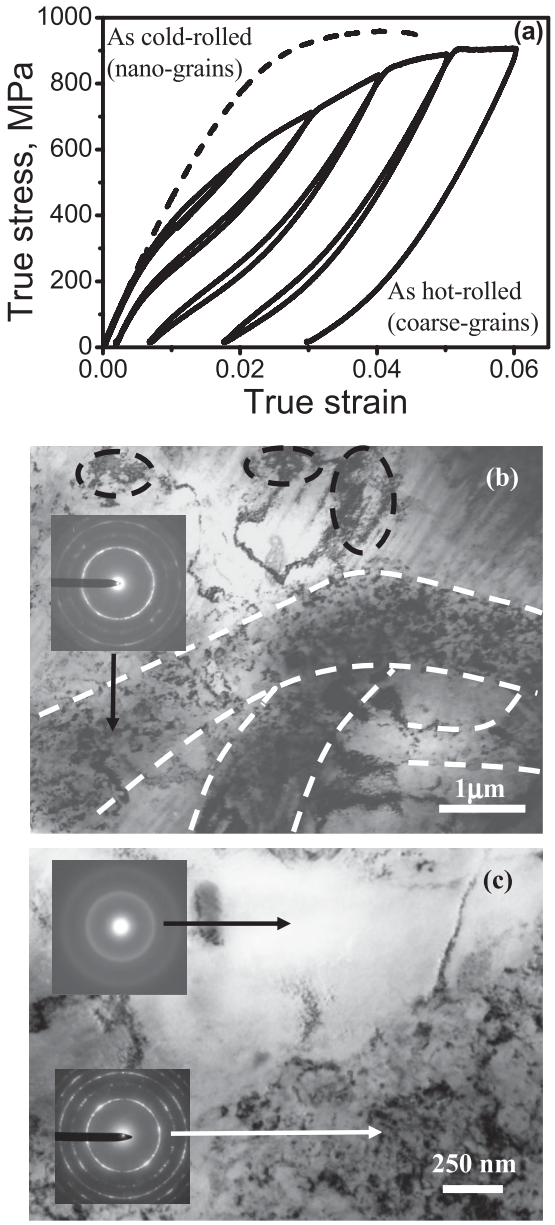

FIG. 3. Deformation behavior of $TiNb_{24}Zr_4Sn_{7.9}$ alloy. (a) Stress-strain curves from a cyclic tensile test of the hot-rolled alloy (solid curve) and of the cold-rolled alloy (dashed curve); (b, c) TEM microstructures of the hot-rolled alloy after 50% compression, showing regions of highly-localized plastic deformation within an original coarse grain that induces the formation of nanocrystal bands (b) and crystalline-amorphous transition (c).

decreased by ~10 GPa after slight cold drawing to area reductions of just about 10 ~ 15%.

The 7.9 wt.% Sn alloy also exhibits peculiar plastic deformation behavior. For specimens with grain size of ~100 μm obtained by heat treatment at 1123 K for 1 h of hot-rolled billet, a 50% compression at a strain rate of ~1 s^{-1} produces regions of highly-localized plastic deformation that span ~1 μm [Fig. 3(b)]. In these regions, the original coarse grain was fragmented into nanocrystals, as evidenced by continual diffraction rings of single β phase on the diffraction pattern [inset of Fig. 3(b)]. The bandlike morphology of these regions promoted us to term them "shear bands" [7]. However, these shear bands contrast with those observed in brittle materials such as nanostructured metallic materials (NMMs) or BMGs in which the shear bands are normally straight and extend significantly to show plank-type morphology [4,9]. In the bcc crystals however they show needlelike morphology and may be severely curved along their length direction [noted by pairs of white curves and black ellipses in Fig. 3(b)]. Clearly these bands do not lie on specific crystallographic planes of the original grain. Outside these nanocrystal bands, there exist slip bands spaced at tens of nanometers. Because the strain rate during compression is relatively large, even amorphous transition can be induced from the bcc crystal by the highly-localized plastic deformation [Fig. 3(c)]. Conventional cold rolling to a thickness reduction of 90% produces uniform nanostructures with grain sizes less than 50 nm, typically in the range of 20–30 nm [7]. Tensile test [Fig. 3(a)] demonstrates that the grain refinement has little strengthening effect and cannot fully suppress the nonlinear elastic deformation behavior.

The above peculiar elastic and plastic behaviors might be explained by assuming the bcc crystal approaching its elastic limit under external stress. Hydrostatic tension or compression of the 7.9 wt.% Sn alloy possessing an ultralow bulk modulus ~24 GPa has significant effect on lattice parameter if the bcc crystal remains stable. As an example, a hydrostatic tension at a stress of 0.6 GPa expands the crystal volume and dilates the lattice parameter by 2.5% and 0.8%, respectively. The lattice dilation results in weaker attractive forces among atoms and reduces the elastic modulus accordingly. This explains the elastic softening with increasing tensile stress as observed in Fig. 3(a). Hydrostatic compression, on the contrary, results in elastic hardening. The low Poisson's ratio of the 7.9 wt.% Sn alloy (Fig. 2) is then a natural result of the elastic softening along the tensile direction but hardening along the lateral directions during tension. The lattice contraction and recovery were confirmed by *in situ* x-ray diffraction (XRD) measurements of plate-shaped samples at different amounts of tensile strain and after unloading [Fig. 4(a)]: the (110) peak shifts continuously to higher angles with increasing tensile strain up to 4% at interval of 1%, corresponding to plane spacing contraction of 0.6%, 0.9%, 1.1%, and 1.2%, respectively. After unloading from the 4% prestrain, the (110) plane spacing recovers almost to its original value.

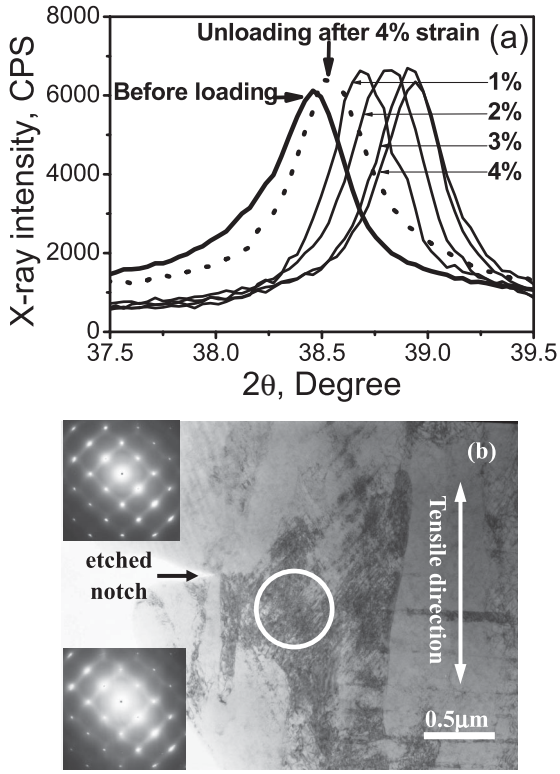

FIG. 4. *In situ* tensile analysis of the hot-rolled $TiNb_{24}Zr_4Sn_{7.9}$ alloy. (a) XRD analysis of a specimen before loading, loaded with strains up to 4% at interval of 1% and unloaded after 4% prestrain, showing $\beta(110)$ peak profiles. (b) Electron diffraction analysis of a sample before and after tensile test to a strain of 2% under TEM. The top and bottom insets show the diffraction patterns before and after straining, respectively, from the circled area in front of a notch formed during foil perforation (foil normal of the grain ~[001]).

These (110) planes from different grains covered by the x-ray scan are at a small angle to the face of the plate-shaped samples and their peak shift to higher angles represents lattice contraction along lateral directions. In Fig. 4(a) the maximum tensile deformation slightly exceeds the limit of the elastic strain of the alloy [~3.3%, see Fig. 3(a)] and the lattice contraction (or dilation) is well understood from the foregoing discussion. In addition, lattice contraction was also observed during heavy cold-rolling. The spacing of the (110) planes approximately parallel to the sheet face in the as hot-rolled state is 0.3299 nm, which reduces to 0.3269 and 0.3264 nm for the 1.5 and 0.45 mm thick sheets obtained by cold rolling to thickness reductions of 90% and 97%, respectively. These contractions of the (110) spacing, ~1%, were measured off load and were held by the large internal stress in the cold-rolled sheets.

According to the relationship between ideal strength of bcc metals and Young's modulus [10], the significant elastic softening during uniaxial tension [Fig. 3(a)] results in an ideal strength of ~1.6 GPa, which is not much higher than the tensile strength of ~0.9 GPa. Such a small difference between ideal and tensile strength limits the room of

strengthening by lattice defects such as dislocations and twins through the Hall-Petch relationship. This is reflected in the fact that the tensile strength is not sensitive to grain refinement as shown in Fig. 3(a), in sharp contrast with previously reported NMMs which normally show several times increase in tensile strength. Such a phenomenon was previously termed ''soft nanostructuring'' [7]. The classical constitutive laws for plasticity as described by the Cosidére criterion [11] dictate that localized deformations will be induced by plastic instability originating from the lack of hardening mechanisms. This is evidenced by the highly localized plastic deformation [Fig. 3(b)] that produces severe plastic strains in local regions to refine grains. Because tensile and compressive stresses have opposite effects on the elastic stability of bcc crystals in the 7.9 wt.% Sn alloy, the elastic softening under the tensile stress results in lattice dilation and atomic shuffle but the elastic hardening under the compressive stress results in lattice contraction. The ultralow bulk modulus of ~24 GPa (Fig. 2) makes the total lattice distortions (including dilation, contraction, and shuffle) much more significant than in other metallic materials with high elastic stability, leading to easy nanostructuring in the highly-localized deformation regions. The character of soft nanostructuring mentioned earlier indicates that no effective barrier exists to hinder the propagation of the nanocrystal bands to the whole specimen. This is the mechanism of grain refinement leading to homogeneous nanostructuring of the alloy during conventional cold rolling [7].

A question that needs to be answered is if a reversible MT contributed to the high recoverable strains as seen in Fig. 3(a). Previous investigations showed that it is possible for elastic instability to induce crystal-crystal transformation and crystalline-amorphous transition [8]. In the present alloy a reversible MT between the β phase and an α'' martensite with orthorhombic crystal structure was indeed observed by XRD analysis of the cold-rolled and compressed bulk samples [7]. This transformation, however, was rarely detected in tensile deformed samples. An *in situ* TEM analysis [Fig. 4(b)] shows that the α'' martensite has not formed even in a stress-concentrated area at 2% tensile strain, as evidenced by the (001) diffraction pattern which shows no characteristic reflections due to the martensite (bottom inset). This is consistent with previous XRD analysis of the tensile fracture surface which detected only single β phase [7]. It is clear that the nonlinear elasticity and recoverable strains of the present alloy are not due to the martensitic transformation. Nonlinear elasticity is also common in the so-called auxetics with negative Poisson's ratio and the kinking nonlinear elastic (KNE) solids such as some geological materials, layered materials, and hexagonal close-packed crystals with large c/a ratios [12]. It was also found in other β-type titanium alloys after severe cold swaging [13]. In these materials a MT is not present, and the nonlinear elasticity is attributed to various mechanisms ranging from incipient kink bands to dislocation-free sliding.

Mechanisms leading to the high strength and excellent ductility of the alloy with such low elastic moduli are not quite understood. It is plausible that dislocation motion is hindered by the destroying of cubic symmetry due to elastic distortion, delaying yielding to higher stress. The interplay of slip and formation of nanocrystal bands that sustains plastic deformation is not yet clear and needs further investigation.

In conclusion, we identified a distinct minimum in bulk modulus and Poisson's ratio at 7.9 wt.% Sn alloy in $TiNb_{24}Zr_4$-Sn alloys. The essentially identical bulk and shear moduli enable easy crystal distortion, causing significant elastic softening in tension and elastic hardening in compression on one hand, and on the other easy formation of nanostructure in conventional range of plastic strain. The unusual elastic properties combined with high strength and good ductility make the alloy viable for a number of engineering applications.

The work was supported in part by NSFC Grants No. 50471074 and No. 50631030 as well as a Chinese MoST Grant No. 2006CB605104.

*Corresponding author.
Electronic address: ylhao@imr.ac.cn

[1] R. S. Lakes, Science **235**, 1038 (1987).
[2] A. Migliori, H. Ledbetter, D. J. Thoma, and T. W. Darling, J. Appl. Phys. **95**, 2436 (2004).
[3] M. W. Barsoum, Prog. Solid State Chem. **28**, 201 (2000).
[4] J. Schroers and W. L. Johnson, Phys. Rev. Lett. **93**, 255506 (2004).
[5] K. Gschneidner *et al.*, Nat. Mater. **2**, 587 (2003).
[6] S. S. Hecker, D. L. Rohr, and D. F. Stein, Metall. Trans. A **9**, 481 (1978).
[7] Y. L. Hao *et al.*, Appl. Phys. Lett. **87**, 091906 (2005); Mater. Sci. Eng. A **441**, 112 (2006); Acta Biomaterialia. **3**, 277 (2007).
[8] J. H. Wang, S. Yip, S. R. Phillpot, and D. Wolf, Phys. Rev. Lett. **71**, 4182 (1993); J. W. Morris and C. R. Krenn, Philos. Mag. A **80**, 2827 (2000); X. D. Ding, T. Suzuki, J. Sun, X. Ren, and K. Otsuka, Mater. Sci. Eng. A **438–440**, 113 (2006).
[9] D. Jia, K. T. Ramesh, and E. Ma, Acta Mater. **51**, 3495 (2003); Q. Wei *et al.*, Acta Mater. **52**, 1859 (2004).
[10] C. R. Krenn, D. Roundy, J. W. Morris, and M. L. Cohen, Mater. Sci. Eng. A **319–321**, 111 (2001); D. M. Clatterbuk, D. C. Chrzan, and J. W. Morris, Acta Mater. **51**, 2271 (2003).
[11] E. W. Hart, Acta Metall. **15**, 351 (1967).
[12] M. W. Barsoum *et al.*, Nat. Mater. **2**, 107 (2003); M. W. Barsoum *et al.*, Phys. Rev. Lett. **94**, 085501 (2005); S. R. Kalidindi, T. Zhen, and M. W. Barsoum, Mater. Sci. Eng. A **418**, 95 (2006).
[13] T. Saito *et al.*, Science **300**, 464 (2003); S. Kuramoto *et al.*, Mater. Sci. Eng. A **442**, 454 (2006); M. Gutkin, T. Ishizaki, S. Kuramoto, and I. A. Ovid'ko, Acta Mater. **54**, 2489 (2006).